JOURNAL OF GEOPHYSICAL RESEARCH, VOL. 93, NO. C7, PAGES 8119–8130, JULY 15, 1988

A Model Study of Potential Sampling Errors Due to Data Scatter Around Expendable Bathythermograph Transects in the Tropical Pacific

MICHAEL J. MCPHADEN,[1] ANTONIO J. BUSALACCHI,[2] JOËL PICAUT,[3] AND GARY RAYMOND[4]

We describe a series of sampling sensitivity experiments to examine potential errors due to data scatter around expendable bathythermograph (XBT) transects in the tropical Pacific. We use a linear, multiple vertical mode model forced with three different monthly mean wind stress sets for the period 1979–1983. The model is sampled along approximately straight lines of grid points corresponding to the mean positions of XBT tracks in the eastern, central, and western Pacific and then sampled again at the dates and locations of actual XBT casts for 1979–1983. Model dynamic heights are calculated with a resolution of 1° of latitude and 1 month, then processed to a monthly mean seasonal cycle and anomalies associated with the 1982–1983 El Niño. When results are compared for the two methods of sampling, the model indicates that data scattered zonally around XBT transects in general can lead to about 2 dyn cm error in dynamic height (equivalent to a 10-m error in model pycnocline displacement) in composite sections of XBT data. This magnitude of error generally does not obscure anomalies associated with the 1982–1983 El Niño or the annual and semiannual harmonics of the mean seasonal cycle in the model, though frequencies higher than the semiannual can be adversely affected. Errors larger than 2 dyn cm occur in regions where XBT sample spacing in the zonal direction is insufficient to resolve Rossby wave variations in the model (for example, from 16°N to 20°N in the central Pacific and from 8°S to 20°S in the eastern Pacific). These conclusions are insensitive to the choice of monthly mean wind stress used to force the model.

1. INTRODUCTION

The Tropical Ocean–Global Atmosphere program (TOGA) is a 10-year multinational program to measure, understand, model, and predict variability in the coupled ocean-atmosphere system on time scales of months to years, with particular emphasis on the El Niño–Southern Oscillation (ENSO) phenomenon. A central oceanographic objective is to develop an observational array with sufficient accuracy and resolution to determine the time dependent variability of upper ocean thermal and current structures. Data from the tropical Pacific ship of opportunity (SOP) expendable bathythermograph (XBT) program [*National Academy of Sciences*, 1986], together with complementary conductivity-temperature-depth (CTD) data, hydrocast data, and XBT data from research and naval vessels, are an important component of this observational effort in that they provide basin-scale temperature information in the upper 450 m.

A number of recent studies have dealt with tropical Pacific thermal sampling issues of relevance to TOGA. For example, *White et al.* [1982] estimated time and space scales and signal-to-noise ratios of climate scale variability from pre-1979 hydrographic data in the western Pacific. This study provided a rationale for the design of an SOP network to detect large-scale interannual variations in thermal structure associated with ENSO. More recently, *Kessler et al.* [1985] have used SOP XBT data to address issues of oversampling in the central Pacific, of the shallow 450-m reference level, and of data loss with increasing depth. *Kessler and Taft* [1987] examined the implications of using a climatological temperature-salinity (T-S) relationship for estimating dynamic height from temperature alone in the central Pacific. *Firing and Lukas* [1985] investigated the effects of aliased high frequencies on central equatorial Pacific temperature data sparsely sampled in time. These and other efforts to define errors inherent in thermal field sampling strategies have made an important contribution to quantitative analyses of existing XBT data.

XBT data are commonly processed for analysis in two ways. One is to grid the data on horizontal planes for mapping [e.g., *White et al.*, 1985], and the other is to group data scattered zonally about major shipping lanes into two-dimensional vertical sections [e.g., *Kessler and Taft*, 1987]. The error associated with grouping scattered data into vertical sections has not yet been evaluated because of limitations in the observational data base. An error analysis using field data would require large numbers of simultaneous casts separated zonally in such a way that temporal aliasing could be ruled out as a source of error. Data separated in time by even a few hours would not satisfy this requirement because of internal wave noise.

The purpose of this study is therefore to use a linear, multiple vertical mode model to examine potential errors involved in grouping zonally scattered data into vertical sections. This model has been used in a study of the mean seasonal cycle for the period 1979–1981 [*McPhaden et al.*, this issue], and similar versions of the model have been used to study the 1982–1983 El Niño [e.g., *Busalacchi and Cane*, 1985; *Inoue et al.*, 1987]. In each case, quantitative agreement was found between observed and modeled sea level, dynamic height, and/or thermocline depth variability. Also, in a similar linear, reduced-gravity model of the tropical Pacific run with monthly winds for the period 1961–1984, M. Kubota and J. J. O'Brien (Variability of the upper tropical Pacific Ocean model, submitted to *Journal of Geophysical Research*, 1987) found meridional decorrelation scales of about 4° latitude and zonal decorrelation scales of typically 10° to 20° of longitude for model pycnocline depth. These are comparable to the scales reported by *White et al.* [1982, 1985] for variations on

[1]NOAA Pacific Marine Environmental Laboratory, Seattle, Washington.
[2]Laboratory for Oceans, NASA Goddard Space Flight Center, Greenbelt, Maryland.
[3]Groupe SURTROPAC, Office de la Recherche Scientifique et Technique Outre-Mer, Nouméa, New Caledonia.
[4]School of Oceanography, University of Washington, Seattle.

Paper number 8C0291.
0148-0227/88/008C-0291$05.00.

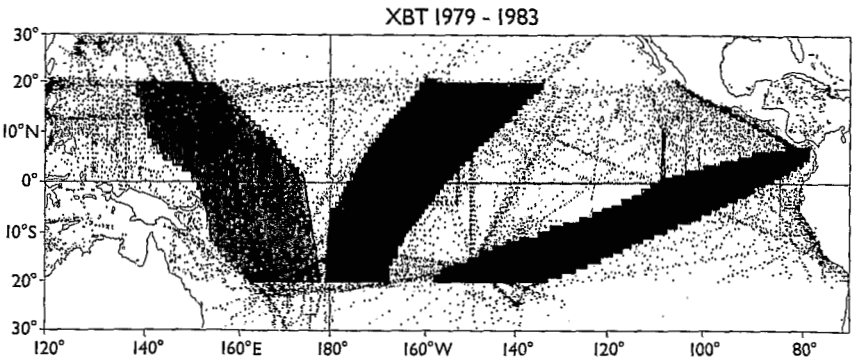

Fig. 1. Distribution of XBT data in the tropical Pacific for the period 1979–1983. Shaded areas indicate groupings of XBT data in the eastern, central, and western Pacific.

seasonal time scales observed in hydrographic and XBT data, so that the model can be used with confidence in a discussion of sampling errors.

We examine the period 1979–1983 because there are several contemporaneous monthly wind products that can be used to force the model and extensive XBT data coverage (Figure 1). The procedure is to sample model integrations at a series of grid points closely approximating straight lines which correspond to the mean positions of XBT transects in the eastern, central, and western Pacific. The model is then sampled at the dates and locations of actual XBT casts in each of the three regions defined in Figure 1. In each case, model data are processed to a mean seasonal cycle and 1982–1983 El Niño anomalies in dynamic height. Differences in the two methods of sampling provide a measure of the potential for error due to zonal scatter about the mean position of the XBT tracks.

This paper is outlined as follows. The XBT data distribution and sampling patterns are described in section 2, followed by a discussion in section 3 of the numerical model and wind forcing used for the sampling experiments. Results of the simulation experiments are presented in section 4, and a summary of major conclusions is presented in section 5. The principal results of this work are that data scatter leads to aliasing of zonal variations which may introduce a 2 dyn cm error in dynamic heights (equivalent to 10-m pycnocline or thermocline displacements) in composite sections of XBT data (though larger errors may occur in regions where ship tracks are separated by 10° or more of longitude). This 2 dyn cm error, which is comparable to other observational errors (e.g., due to use of mean T-S relationship or to the aliasing of internal waves) should not obscure detection of El Niño anomalies or of annual and semiannual harmonics in the mean seasonal cycle. Frequencies higher than the semiannual, however, may be adversely affected.

2. XBT Data

Figure 1 shows the distribution of nonredundant, research quality thermal data available to the TOGA community in the tropical Pacific for the period 1979–1983. The total number of casts is close to 35,000, which includes the SOP XBT data, additional XBT data from national hydrographic offices and navies, and some CTD and hydrocast data (J. Picaut et al., manuscript in preparation, 1988 (hereinafter referred to as Picaut et al., 1988)). Many of these data are concentrated along well-traveled shipping lanes in the eastern Pacific, central Pacific, and western Pacific. For the period 1979–1983, the regions outlined in Figure 1 contain a total of 18,565 XBT casts of which 4550 are in the eastern, 8229 in the central, and 5786 in the western Pacific. Data have been grouped without regard to longitude in these regions, producing data densities of 2.8, 3.3 and 2.4 XBTs per month per degree latitude, respectively. These regions have been defined subjectively for other studies [e.g., *McPhaden et al.*, this issue; Picaut et al., 1988] so that they contain at least one XBT per month per degree of latitude, though other groupings are possible [e.g., *Kessler and Taft*, 1987]. Within each region there is a spread of data in the longitudinal direction, however. Most of the data in the western Pacific tend to be concentrated along a single track between Nouméa and Japan for the 1979–1983 period covered in this study. Data in the cental Pacific are spread across two broad swaths which intersect around 10°S, 175°W, but which are separated by more than 20° of longitude at 20°N. In the eastern Pacific, two heavily traveled tracks diverge south of the equator and are separated by more than 10° of longitude by 10°S.

Figure 2 shows surface dynamic height relative to 400 dbar calculated by averaging data from 1979–1983 along the central Pacific track into bins of 1° latitude and 1 month. Dynamic height has been calculated using XBT temperatures and mean T and S from *Levitus* [1982]. We present these data for a brief comparison with model simulated dynamic height in section 4. More extensive discussion of the data can be found in the paper by *McPhaden et al.* [this issue].

Figures 2*a*–2*d* show the mean seasonal cycle for 1979–1981, the annual mean for 1979–1981, seasonal variations about the annual mean, and the standard deviation of mean seasonal cycle, respectively. In the central Pacific, the North Equatorial Countercurrent (NECC) trough is located on average at 10°N (Figure 2*b*), and is shallowest in boreal spring and deepest in boreal fall (Figure 2*a*). There is an equatorial ridge at 5°N and an equatorial trough centered on the equator. Variability in the vicinity of the equatorial ridge and trough is in phase, with low sea level in boreal spring and early summer and high sea level in boreal fall (Figure 2*c*). A South Equatorial Countercurrent (SECC) ridge near 8°S is highest in boreal spring and lowest in boreal fall. A typical standard deviation of monthly means across 20°N to 20°S is 2–3 dyn cm, with values of 5–6 dyn cm in the vicinity of the NECC trough and equatorial ridge (Figure 2*d*). Currents associated with this ridge-trough topography are the North Equatorial Current (NEC) north of

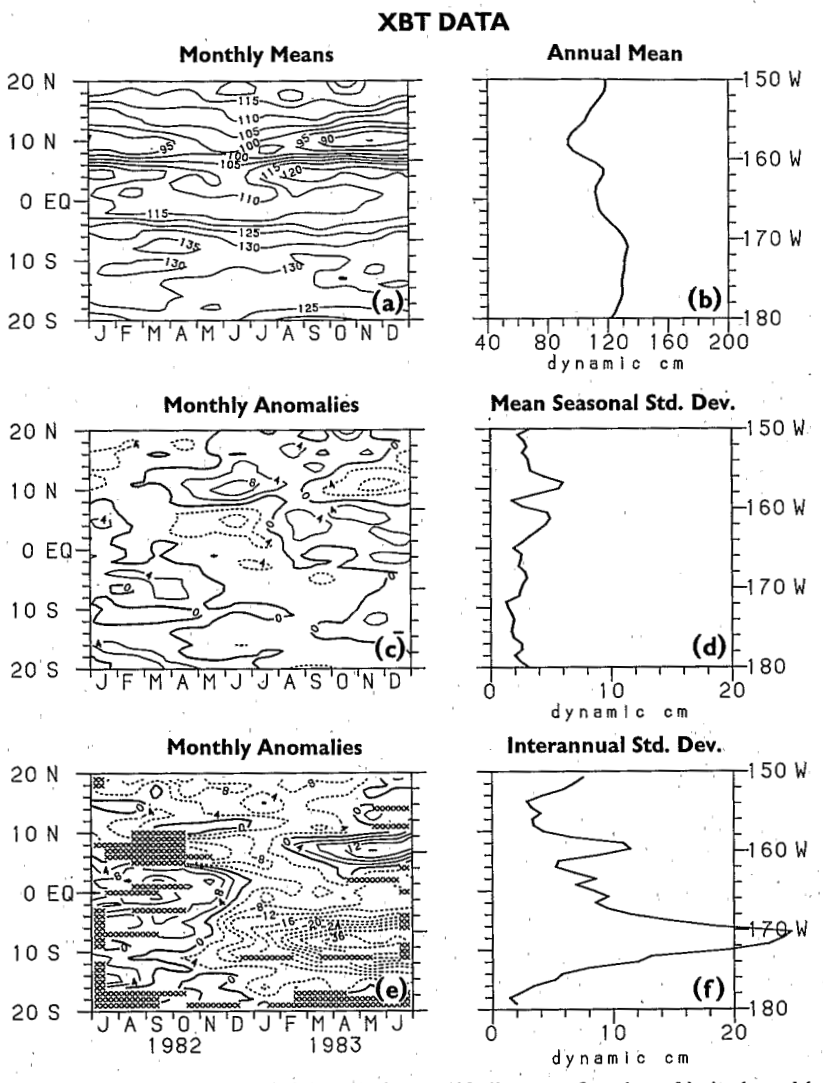

Fig. 2. XBT data processed to dynamic heights relative to 400 dbar as a function of latitude and longitude from the central Pacific swath of data in Figure 1 for the period 1979–1983; (*a*) Monthly means, (*b*) annual mean, (*c*) monthly anomalies computed as the difference of the annual mean from the monthly mean, (*d*) mean seasonal standard deviation computed from monthly anomalies, (*e*) El Niño anomalies of July 1982 through June 1983 from the mean seasonal cycle, and (*f*) standard deviation of the El Niño anomalies. The contour interval is 5 dyn cm in Figure 2*a* and 4 dyn cm in Figures 2*c* and 2*e*. Cross hatching in Figure 2*e* indicates that no XBT data were available.

10°N, the NECC between 5°N and 10°N, the South Equatorial Current (SEC) between 5°N and 8°S and the South Equatorial Countercurrent (SECC) between 8°S and 12°S in boreal spring.

Figure 2*e* shows El Niño anomalies of July 1982 through June 1983 from the 1979–1981 mean seasonal cycle, and Figure 2*f* shows their standard deviation. For our purposes it is important to note that El Niño anomalies, which often exceed 10 dyn cm, are larger in general than variations in the mean seasonal cycle, particularly between 5° and 10°S. *Kessler and Taft* [1987] find similar variations in dynamic topography in the central Pacific using an XBT data set similar to ours, but with about 35% fewer data during 1979–1983.

3. Model and Wind Forcings

The model used in this study is similar to that employed by *Busalacchi and O'Brien* [1980]. A linear, numerical treatment of the shallow water wave equations is used here to address sampling questions with respect to the wind-driven dynamic response of the tropical Pacific Ocean. Changes to the previous verison of the model include increased horizontal resolution of 40 km between like variables and a horizontal Laplacian friction of 10^7 cm^2 s^{-1}. The model basin extends from 20°N to 20°S and 126°E to 70°W. A no-slip condition is imposed along the idealized coastal boundaries, and an open boundary condition [*Roed and Smedstad*, 1984] is applied at the northern and southern boundaries. Model height field solutions are generated for the four gravest baroclinic modes of a specific Brunt-Väisälä profile. A final solution is found by summing the individual contributions of all four modes. The modal decomposition, based on stratification data between 1.5°N and 1.5°S at 179°W as presented by *Eriksen et al.* [1983], is also the same as that used by *Cane* [1984] and *Busalacchi and Cane* [1985]. These data were chosen because they were obtained within the equatorial waveguide in a region with significant wind stress fluctuations on seasonal

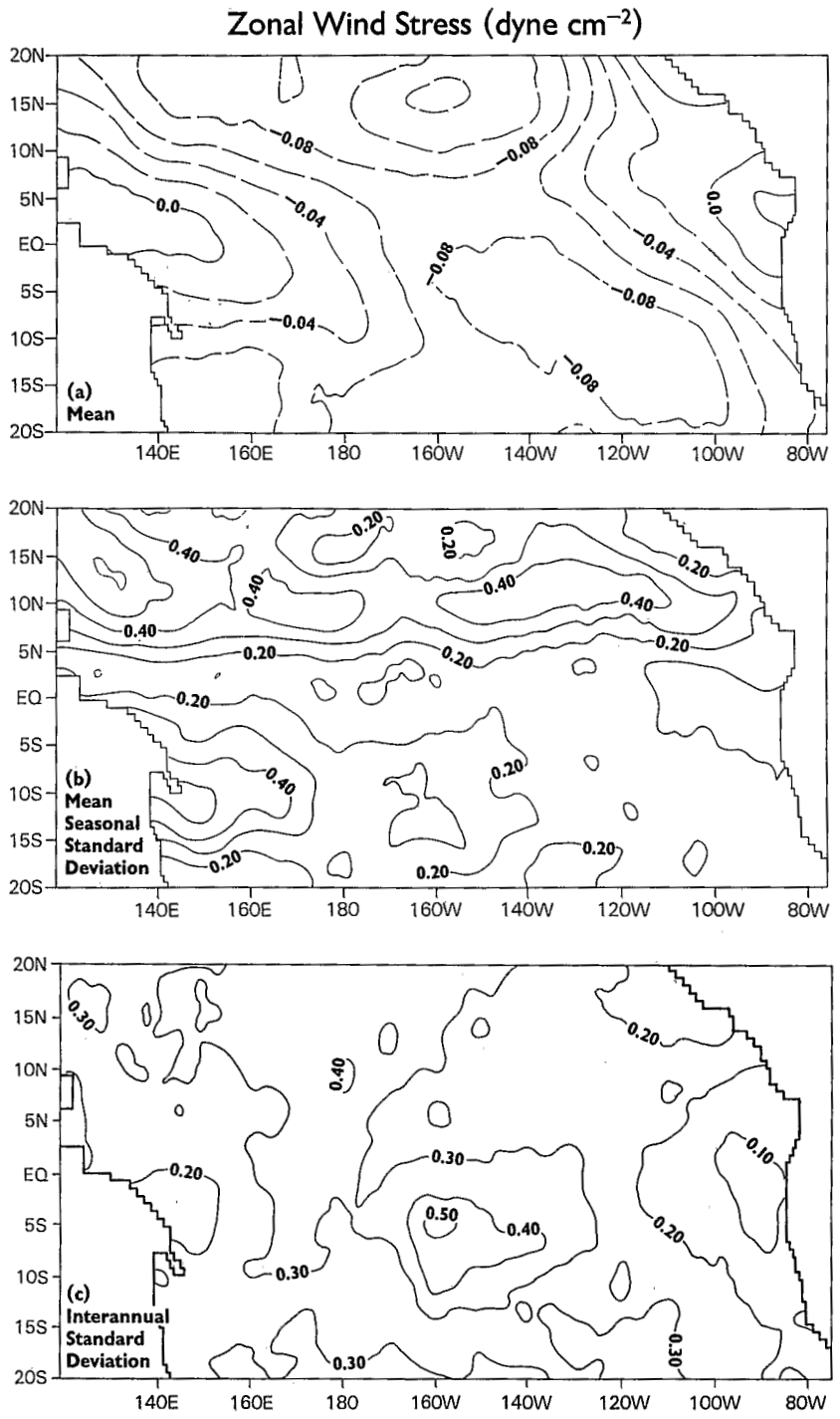

Fig. 3. FSU zonal wind stress (in dyn cm^{-2}): (*a*) mean for 1979–1981, (*b*) standard deviation of the mean seasonal cycle for 1979–1981, and (*c*) standard deviation of 1979–1983 anomalies about the mean seasonal cycle. Dashed contours in Figure 3*a* indicate westward wind stress.

and interannual time scales. The internal wave speeds for the four vertical modes are $c_1 = 2.90$ m s^{-1}, $c_2 = 1.77$ m s^{-1}, $c_3 = 1.13$ m s^{-1}, and $C_4 = 0.84$ m s^{-1}.

Because of the range of the four wave speeds, the time step of the model is mode dependent. All mode 1 calculations have a 1-hour time step, whereas the slower speeds of modes 2–4 permit a 2-hour time step without compromising numerical stability. Similarly, the time required for initial transients to die out during spin-up is mode dependent. Beginning from a state of no motion and in response to a mean seasonal wind stress for 1979–1981, an exact repeating seasonal cycle is obtained basin-wide after a spin-up of 12 years for mode 1, 22 years for mode 2, 42 years for mode 3, and 62 years for mode 4. After the seasonal cycle has spun up, the u, v, and h fields at the end of the mean seasonal year are used as the initial conditions for a 5-year integration forced by individual monthly mean wind stresses for 1979 through 1983.

The model integrations are performed using three different

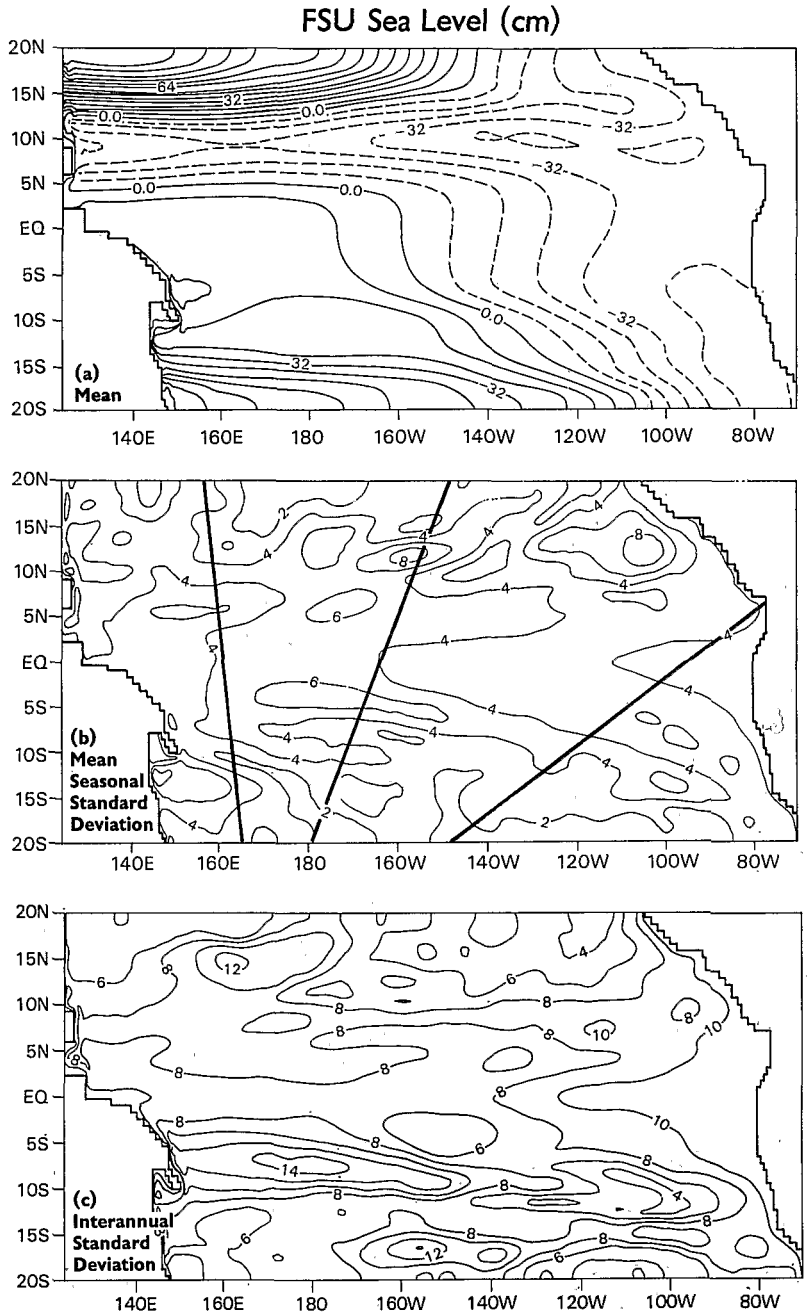

Fig. 4. Model sea level response to FSU wind forcing (in centimeters): (*a*) mean for 1979–1981, (*b*) standard deviation of the mean seasonal cycle for 1979–1981, and (*c*) standard deviation of 1979–1983 anomalies about the mean seasonal cycle. Solid (dashed) contours in Figure 4*a* indicate elevated (depressed) sea level relative to an ocean at rest. Heavy lines in Figure 4*b* indicate the approximate mean position of XBT distributions in the eastern, central, and western Pacific.

wind stress products for which monthly means are currently available for January 1979 through December 1983. Two of these data sets are derived from subjective analyses, and the third is derived from an operational objective analysis. One of the subjective analysis is the Florida State University (FSU) analysis of ship wind observations provided by J. J. O'Brien. The analysis procedure of transforming individual shipboard observations into monthly mean wind stress fields on a $2° \times 2°$ grid is described by *Goldenberg and O'Brien* [1981]. The other subjective analysis (referred to as UH) is a combination of satellite-observed, low-level cloud motion vectors, ship wind observations, island wind observations, and buoy wind observations performed by J. Sadler at the University of Hawaii. The derivation of monthly mean surface wind and wind stress on $2.5° \times 2.5°$ grid is described by *Sadler and Kilonsky* [1985] and *Sadler et al* [1987]. The third data set we use is an objectively analyzed operational product from the Global Band Analyses of the U.S. Navy's Fleet Numerical Oceanography Center (FNOC). An objective analysis based on *Cressman* [1959] is used on all reports (ship, island, buoy, etc.) in an operational data base for 6-hour intervals on a $2.5° \times 2.5°$ grid. Six-hourly stresses are computed and averaged to form the monthly means used here. In the present study a constant drag coefficient of 1.5×10^{-3} is used to con-

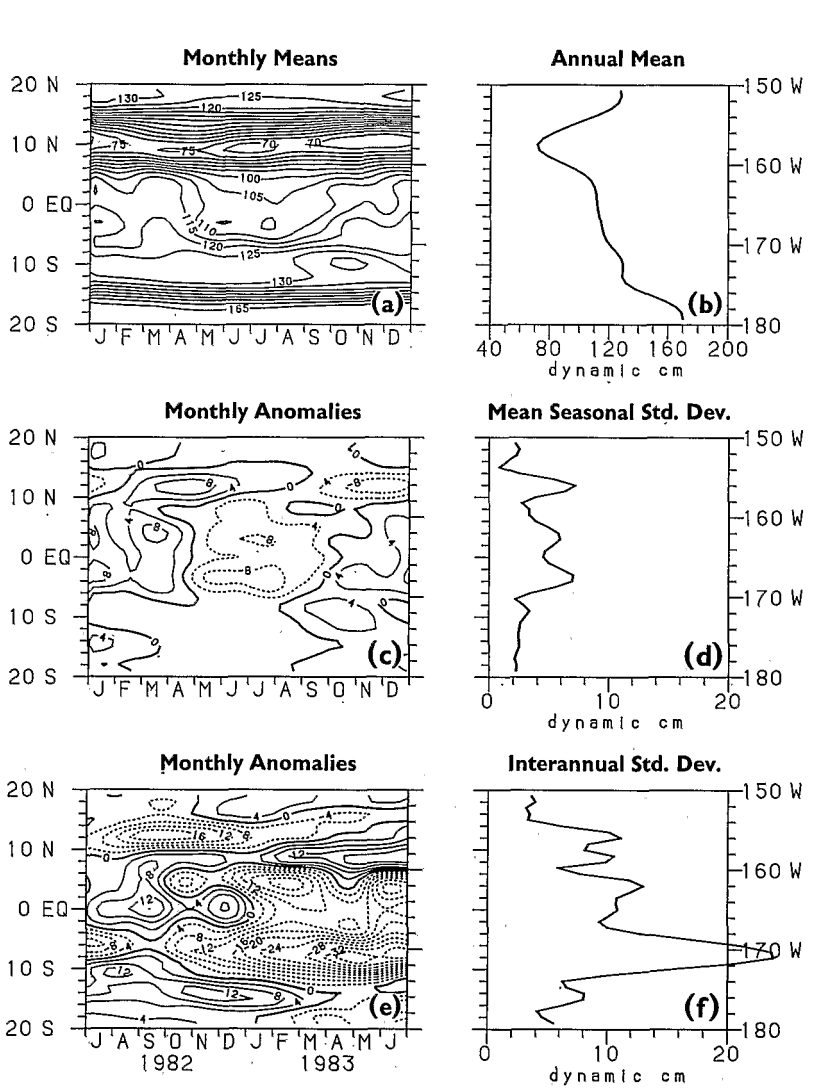

Fig. 5. Dynamic heights relative to 400 dbar as in Figure 2, but for the central Pacific grid point transect from the model forced by FSU winds for the period 1979–1983.

vert from wind to wind stress for each of the three wind data sets.

The 1979–1981 mean zonal wind stress from the FSU analysis is shown in Figure 3*a*. The easterly component of the northeast and southeast trade winds is predominant over most of the basin. Quite evident are the core regions (>0.8 dyn cm^{-2}) of the trades poleward of 10°. Weak mean westerlies are present at low latitudes at the extreme ends of the basin. In general, similar mean features are present in the UH and FNOC fields. The standard deviation of the mean seasonal cycle for 1979–1981 is shown in Figure 3*b*. Zonal wind stress fluctuations over this 3-year period are smallest within 5° of the equator and in the southeastern tropical Pacific. The largest fluctuations (>0.4 dyn cm^{-2}) occur off the equator, where gradients in the mean zonal wind stress are largest, and also within the monsoon regimes of both hemispheres in the west. Basin-wide, 60–80% of this mean seasonal variability is due to the annual harmonic. The standard deviation of zonal wind stress anomalies about the mean seasonal cycle is shown in Figure 3*c*. Variations are dominated by the extreme anomalies associated with the 1982–1983 El Niño. The largest variability occurs near and south of the equator in the central Pacific in regions where the mean seasonal fluctuations are generally small (compare Figure 3*b*). Similar large-scale features of the variability are present in the UH and FNOC analyses as well.

The mean 1979–1981 sea level modeled in response to the FSU wind forcing is presented in Figure 4*a*. The sea level distribution is characterized by a system of zonally oriented troughs and ridges delineating the major geostrophic currents of the model solution. Between the sea level ridge at 20°N and the trough at 9°N flows a westward directed North Equatorial Current. An eastward flowing North Equatorial Countercurrent is flanked by the North Equatorial Countercurrent trough to the north (9°N) and an equatorial ridge to the south (2°–4°N). Considerably less structure is found in the southern hemisphere, where a weak South Equatorial Current is found between 6° and 20°S. Mean seasonal fluctuation are summarized by a standard deviation of the variability for 1979–1981 (Figure 4*b*). As in the winds, 60–80% of the variance is associated with the annual harmonic. The largest seasonal changes (>8 cm) occur in the northeastern corner of the basin in a region known as the Costa Rica dome. Further to the west,

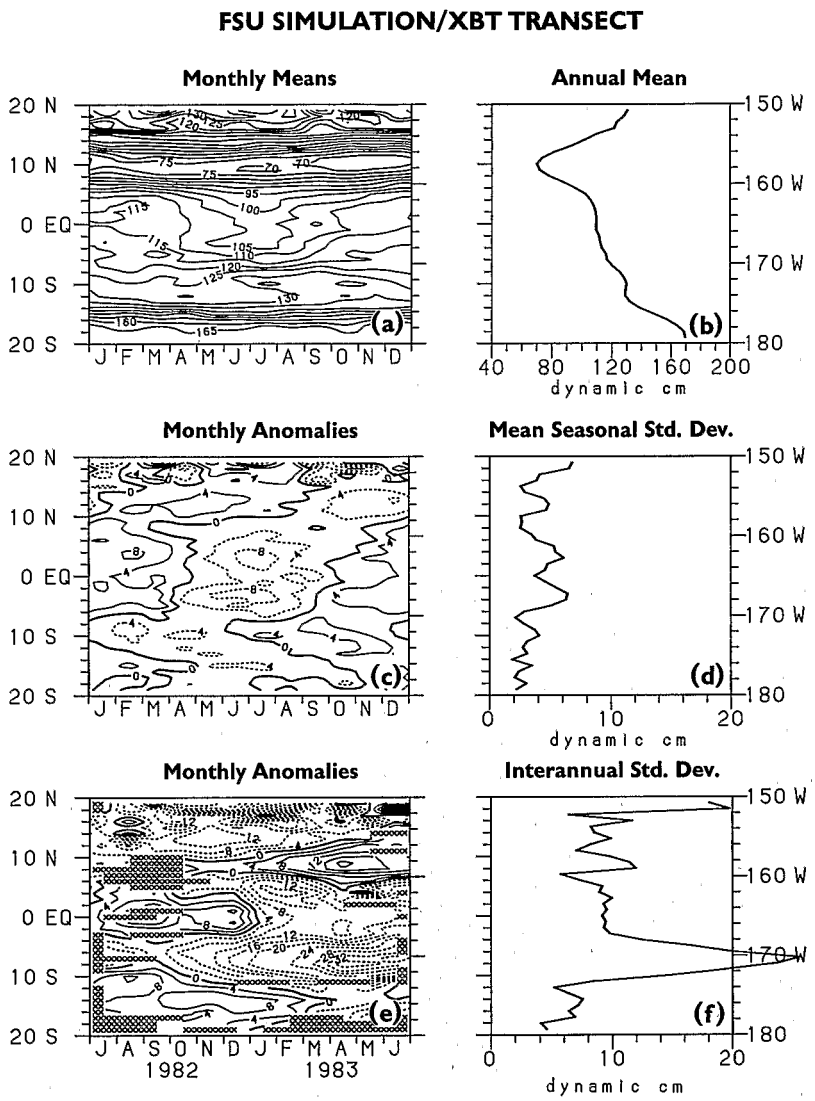

Fig. 6. Dynamic heights relative to 400 dbar as in Figure 5, but for the central Pacific model XBT transect.

most of the dominant variability is found within the same latitudinal band of 10°–15°N, resulting in seasonal changes to the NEC-NECC system. Maxima in the southern hemisphere are representative of seasonal changes to the South Equatorial Current and the reversal and intensification of a South Equatorial Countercurrent. The pattern of interannual fluctuations about the mean seasonal cycle, which is dominated by the 1982–1983 El Niño, is shown in Figure 4*c*. The variations are stronger in general than for the mean seasonal cycle and have a somewhat different pattern. Variations in excess of 10 cm rms occur east of 120°W between 10°N and 10°S, and west of 160°W between 10° and 15°N and between 5° and 10°S.

4. Results of Sampling Experiments

The results presented in this section are derived from sampling the model in two different ways. The first is to extract data from the model along "grid point transects," i.e., from approximately straight lines of grid points in the model that correspond to the mean position of XBT tracks in the eastern, central, and western Pacific. Grid point transects are superimposed on the sea level standard deviation plot in Figure 4*b*. A mean seasonal cycle for 1979–1981, as well as the July 1982 through June 1983 anomalies from this seasonal cycle, are then computed at each degree of latitude. The second method of extracting data from the model is to sample at the exact dates and latitude-longitude positions of actual XBT casts during 1979–1983. Data are then binned by month and by degree of latitude in each of the three regions outlined in Figure 1 for computation of a mean seasonal cycle and El Niño anomalies. Data density in time (2.8–3.3 XBTs per month per degree latitude) is sufficient to resolve the highest model frequency of 1 cycle per 2 months, so that any differences between these "XBT transects" and the corresponding grid point transects result from aliasing of zonal variations in the model. For consistency with XBT measurements, model dynamic heights are computed relative to 400 dbar, though the correlation between model sea level and dynamic heights is high as is the correlation between observed sea level and dynamic heights in the tropics [e.g., *Rebert et al.*, 1985].

Figure 5 shows variations along the grid point transect taken from the central Pacific in the model. We note that as in the observations (Figure 2), the NECC trough is located near

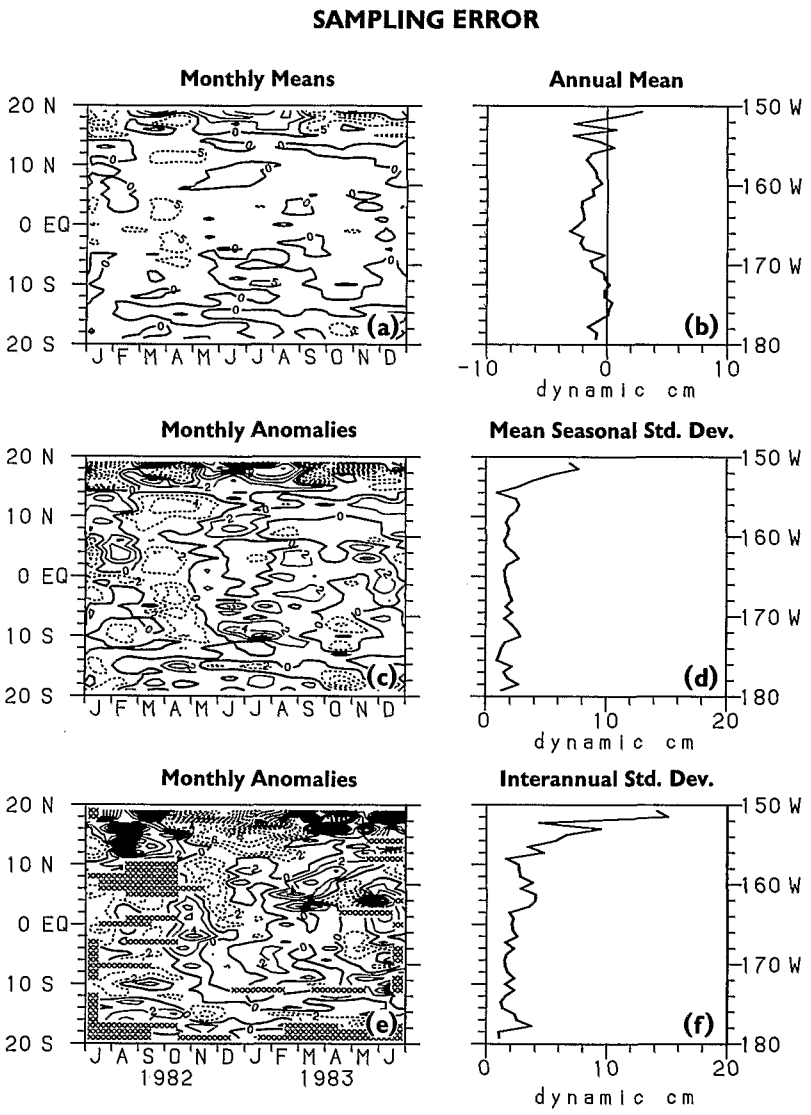

Fig. 7. The dynamic height difference field obtained by subtracting the grid point transect from the XBT transect. Figures 7*a*–7*e* are as defined in Figure 2. The contour interval is 5 dyn cm in Figure 7*a* and 2 dyn cm in Figures 7*c* and 7*e*.

10°N (Figure 5*b*), and is shallowest in boreal spring and deepest in boreal fall (Figure 5*a*). Similarly, near the equator, dynamic height is low in spring and summer and high in winter. Variations are comparable in magnitude to those in the XBT data shown in Figure 2, with a maximum just north of the NECC trough of 7 dyn cm and another maximum near 3°N (2° latitude south of the corresponding maximum in the data) of 5 dyn cm. Anomalies in 1982–1983 (Figures 5*e* and 5*f*) are generally stronger than variations in the mean seasonal cycle, especially between 5° and 10°S in the first part of 1983 when there is a very large depression of 20–30 dyn cm in surface elevation similar to that seen in Figure 2*e*. There are significant differences between the data sets, however, which are elaborated on by *McPhaden et al.* [this issue]. The model has very high north and south equatorial ridges at 20°N and 20°S and no mean equatorial trough. Also, the model section contains a maximum in dynamic height variability near 4°S which is absent in the data. Finally, the SECC ridge is best developed in boreal fall near 10°S in the model as compared with near 8°S in boreal spring in the data. Thus as expected, the model is an imperfect analogue of the real ocean, though the model variability has many features in common with that inferred from XBT data. We proceed with a sampling sensitivity study with these limitations in mind.

Figure 6 shows the effect of sampling the model at XBT times and locations. Most of the major features evident in the grid point transect are evident in the XBT transect (for example, the seasonal variations in the NECC trough and along the equator). However, there is a significant amount of small-scale noise introduced into the analysis due to aliasing of zonal variations around the mean position of the XBT transect. The most noticeable effects of this noise are a reduction in amplitude of mean seasonal variations near 12°N and very large amplitude fluctuations between 16°N and 20°N. Figure 7 shows the noise field more clearly, where we have defined noise as the difference between the XBT transect minus the grid point transect time series. (The difference during 1982–1983 is the difference of the total dynamic height time series, not the anomaly time series, since differences of the latter include differences of the mean seasonal cycle). The error on average is about 2 dyn cm for both the mean seasonal cycle and the El Niño period, except between 16°N and 20°N where

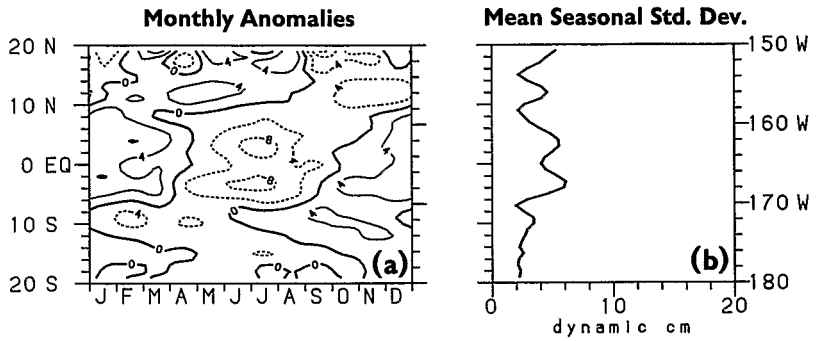

Fig. 8. Dynamic heights from the model XBT transect in Figure 6 smoothed with a 1-2-1 latitudinal filter: (*a*) deviations from annual mean and (*b*) mean seasonal standard deviation.

in both cases it rises well above 4 dyn cm. The reason for this large error in the northernmost portion of the XBT transect is that the data are collected along two broad swaths separated by more than 20° of longitude. At this separation, first vertical mode Rossby waves at the annual period, which are an important source of variability at these latitudes in the model, are badly aliased because their zonal wavelengths are only about 17° of longitude.

Noise levels in the XBT transect can be reduced slightly by averaging in latitude and/or time. Figure 8, for example, shows the effects of passing a 1-2-1 filter over the mean seasonal data in the latitudinal direction at one degree intervals. Variations in dynamic topography are smoother than in the XBT transect in Figures 6*c* and 6*d* and features corresponding to the grid point transect in Figure 5 are better defined. However, noise levels are still about 2 dyn cm in amplitude. Moreover, smoothing does not recover the signal amplitude at 12°N, nor does it eliminate the noise variance between 16°N and 20°N.

Comparison of Figures 5 and 7 suggests that noise due to data scatter is more of a problem for detection of typical seasonal variations than for El Niño anomalies. Mean seasonal variations are of smaller amplitude than El Niño variations, but noise levels are comparable for both (except between 16°N and 20°N). We thus examine the limits of detectability in greater detail for seasonal variations. Figure 9 shows model frequency spectra of mean seasonal dynamic height variance averaged over all latitudes in the central Pacific. Figure 9*a* shows the total variance for the grid point transect, the XBT transect, the XBT transect smoothed in latitude with a 1-2-1 filter and the XBT transect smoothed in time with a monthly 1-2-1 filter. The spectra are red with most variance at 1 cycle

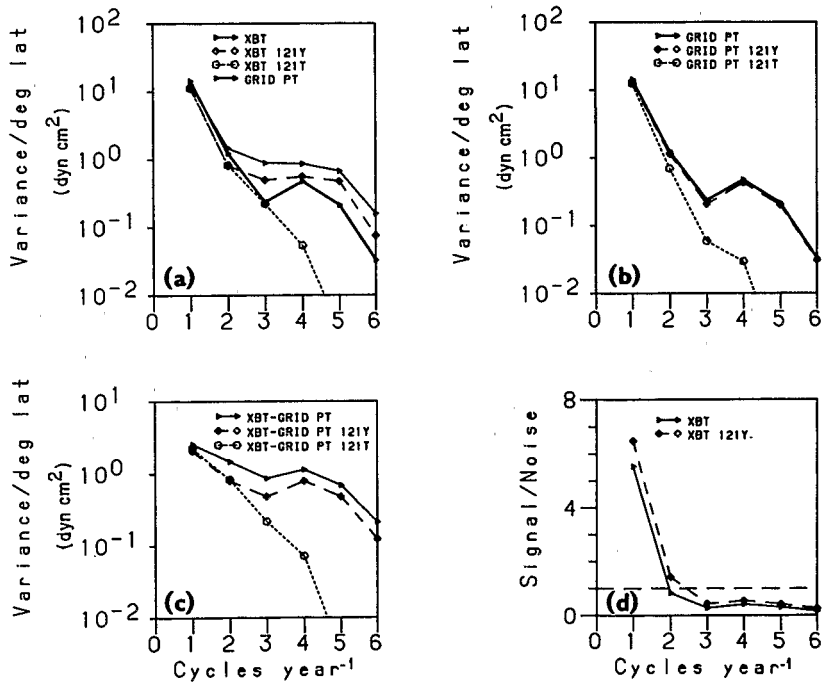

Fig. 9. (*a*) Latitudinally averaged dynamic height variance relative to 400 dbar (in dynamic cm^2) as a function of frequency for the grid point transect, the XBT transect, the XBT transect smoothed in latitude with a 1-2-1 filter (i.e., 121*Y*) and the XBT transect smoothed in time with a 1-2-1 monthly filter (i.e., 121*T*): (*a*) total variance, (*b*) signal variance, and (*c*) noise variance due to zonal aliasing and (*d*) a signal-to-noise spectrum computed as a ratio of spectral coefficients in Figure 9*b* to those in Figure 9*c*.

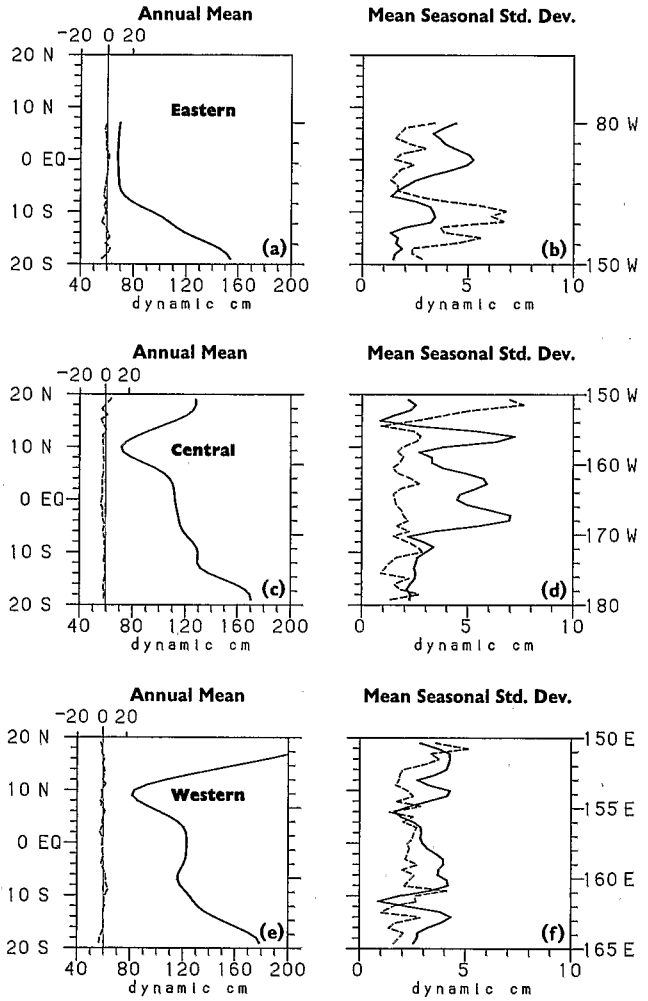

Fig. 10. Dynamic height annual means and mean seasonal standard deviations relative to 400 dbar (in dynamic centimeters) from grid point transects in the eastern, central, and western Pacific (solid lines) superimposed on noise due to zonal aliasing in XBT transects (dashed lines).

per year (cpy) in each case. Energy levels in the XBT transect are higher at all frequencies compared with the grid point transect owing to small-scale noise. Smoothing in latitude and/or time reduces variance levels at the higher frequencies where this noise is most prominent. Figures 9*b* and 9*c* separate the signal and noise components of the total spectra in Figure 9*a*. Smoothing in latitude does not remove much signal variance, whereas noise levels are reduced uniformly in frequency. Conversely, smoothing in time eliminates the highest frequencies in both the signal and noise spectra.

Signal-to-noise variance ratios for the XBT transect and the XBT transect smoothed in latitude are shown in Figure 9*d*. Signal to noise for the XBT transect smoothed in time is identical to that for the unsmoothed XBT transect because both signal and noise are reduced in proportion to one another. Signal-to-noise variance ratios at 1 cpy are 5.6 for the XBT transect and 6.7 for the latitudinally smoothed version of the XBT transect. This ratio drops to near unity at 2 cpy and is less than 0.5 for all higher frequencies.

Thus we can conclude from Figure 9 that zonal aliasing due to data scatter affects all frequencies in monthly mean time series and that it most severely impacts frequencies higher than 1 cpy. Signal-to-noise variance drops below unity at 2 cpy, which marks the probable limits of accurate frequency resolution. Smoothing in time leads to lower overall noise levels than smoothing in latitude, while the latter leads to higher signal-to-noise ratios at low frequencies which contain most of the signal variance.

Figure 10 presents plots of the annual mean and standard deviation of model dynamic height along transects in the eastern, central, and western Pacific. Both signal amplitudes and noise amplitudes are presented for comparison. We see that like the central Pacific, data scatter in general introduces about a 2 dyn cm error in the eastern and western Pacific. Estimates of mean dynamic topography are relatively unaffected, and signal amplitude for the mean seasonal cycle is generally greater than noise amplitude by a factor of 2. Areas where the noise amplitude rises significantly above 4 dyn cm are found between 16°N and 20°N in the central Pacific as noted above, and in the eastern Pacific between 8°S and 16°S. Noise amplitude is also consistently higher than the signal amplitude in both these regions (extending to 20°S in the east) where XBT data are collected along shipping lanes separated by about 10° of longitude or more (Figure 1). In the model, these regions are strongly affected by Rossby wave radiation at 1 cpy which is badly aliased by the sampling distribution of XBT data.

The sampling sensitivity studies discussed above were repeated for the model driven by the UH and FNOC wind products. Figure 11 shows the noise levels in dynamic height for the mean seasonal cycle in the central Pacific. All three model results show a mean and standard deviation noise level of 1–3 dyn cm except between 16°N and 20°N, where errors can be 4 dyn cm or more. The FNOC calculation tends to show slightly lower noise levels along this transect between 15°N and 15°S, though this is not true in general in the eastern and western Pacific. Thus our basic results are insensitive to which wind set is used to force the model.

5. SUMMARY AND CONCLUSIONS

In the preceding sections we described a series of sampling sensitivity experiments to examine potential errors due to data scatter around XBT transects in the tropical Pacific Ocean on estimates of mean seasonal and El Niño dynamic height variations. We have used a linear, multiple vertical mode model forced with three different monthly mean wind stress sets for the period 1979–1983. The model is sampled at approximately straight lines of grid points corresponding to the mean positions of XBT tracks in the eastern, central, and western Pacific and then sampled again at the dates and locations of actual XBT casts for 1979–1983. Model data are processed to a mean seasonal cycle and El Niño anomalies in dynamic height with a resolution of 1° in latitude and 1 month in time. Comparing results for the two methods of sampling indicates that data scatter in general may lead to about an error of 2 dyn cm in dynamic height in composite XBT sections due to aliasing of zonal variations about the mean position of the XBT transects. The error in dynamic height translates into about a 10-m pycnocline displacement in the model. In general, salinity has a secondary effect on density stratification in the tropics, so that these pycnocline displacements would be mirrored in thermocline displacements.

The 2 dyn cm error is comparable to the error that results in the ocean from unresolved internal gravity waves [*Hayes*,

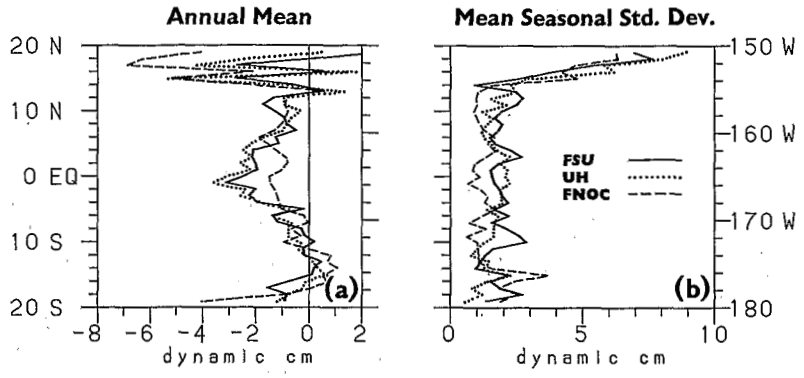

Fig. 11. Noise in dynamic height relative to 400 dbar due to zonal aliasing in the central Pacific for the model driven by FSU (solid lines), UH (dotted lines), FNOC (dashed lines) wind fields: (*a*) annual mean and (*b*) mean seasonal standard deviation.

1982], as is the equivalent 10-m error in thermocline displacement [e.g., *Munk*, 1981]. This error is also comparable to the error of 1–2 dyn cm expected from using a mean T/S relationship to estimate dynamic heights from XBT data [*Kessler and Taft*, 1987]. This magnitude of error generally does not obscure detection of the 1982–1983 El Niño signal or of the weaker mean seasonal cycle in the model. Exceptions to this generalization occur in regions where XBT sample spacing in the zonal direction is insufficient to resolve Rossby wave variations in the model. Specific sites of severe aliasing are 16°N to 20°N in the central Pacific and 8°S to 20°S in the eastern Pacific. Smoothing in latitude and/or time can reduce noise levels slightly but cannot eliminate the effects of aliased zonal variations. In the model we also found that detection of the mean seasonal cycle was limited to 1- and 2-cpy variations, since at higher frequencies signal-to-noise ratios dropped below unity. Thus caution should be exercised in drawing conclusions at frequencies higher than 2 cpy from XBT data grouped along transects as in Figure 1. These results are insensitive to the choice of wind forcing used in the model, since comparable noise levels and patterns appear in simulations forced by the FSU, UH, and FNOC winds.

We performed a similar set of calculations for geostrophic transport per unit width over 0 to 400 m. Transports were calculated orthogonal to each transect for latitudes poleward of 2°N and 2°S. In the mean, the largest transport errors occurred equatorward of 10°, where the geostrophic calculation is most sensitive to small-amplitude dynamic height fluctuations. Both here and at higher latitudes, however, mean errors were relatively small and did not obscure the main features of the mean circulation. Errors in time-varying transport were about 10 $m^2\ s^{-1}$ (equivalent to 5 cm s^{-1} over 200 m), with larger values near the equator and smaller values at higher latitudes. The signal-to-noise amplitude ratio was typically closer to unity, which is lower than that for dynamic height. This is consistent with the fact the transport is a spatial derivative and therefore a high-pass-filtered version of dynamic height. Dynamic height variations tend to be most energetic on large space scales whereas noise variations tend to be white in wave number space. Hence signal-to-noise is less favorable on the smaller scales on which transport variations occur.

The fact that the model used in this study is linear and forced by monthly winds means that it can simulate only frequencies lower than 6 cpy. It is known that there is significant energy at higher frequencies in the tropics due to instabilities of the large-scale current system [e.g., *Legeckis et al.*, 1983], wind forcing [e.g., *Wunsch and Gill*, 1976], and tidal forcing [e.g., *Weisberg et al.*, 1987]. To the extent that these higher frequencies can have zonal scales comparable to or smaller than the XBT sample spacing, as is the case for instability waves with O(100 km) zonal scales, our results probably underestimate the sampling errors due to data scatter in composite XBT sections.

Acknowledgments. The authors would like to thank J. J. O'Brien for providing the FSU wind product, J. Sadler for providing the UH product and J. C. Kindle for providing the FNOC wind product for this study. Support for this work was provided by NOAA's U.S. TOGA Project Office and Equatorial Pacific Ocean Climate Studies (EPOCS) program (M.J.M. and G.R.), by NASA research task operating plan 161-20-31 and Jet Propulsion Laboratory contract 957647 (A.J.B.) and by Office de la Recherche Scientifique et Technique Outre-Mer (ORSTOM) and Programme National de la Dynamique du Climat (PNEDC) (J.P.). We also thank D. Allison, R. Rosario, and V. Fabre for technical assistance. NOAA Pacific Marine Environmental Laboratory contribution 963.

REFERENCES

Busalacchi, A. J., and M. A. Cane, Hindcasts of sea level variations during the 1982–83 El Niño, *J. Phys. Oceanogr.*, *15*, 213–221, 1985

Busalacchi, A. J., and J. J. O'Brien, The seasonal variability in a model of the tropical Pacific, *J. Phys. Oceanogr.*, *10*, 1929–1951, 1980.

Cane, M. A., Modeling sea level during El Niño, *J. Phys. Oceanogr.*, *14*, 1864–1874, 1984.

Cressman, G. P., An operational objective analysis system, *Mon. Weather Rev.*, *87*, 367–374, 1959.

Eriksen, C. C., M. B. Blumenthal, S. P. Hayes, and P. Ripa, Wind-generated equatorial Kelvin waves across the Pacific Ocean, *J. Phys. Oceanogr.*, *13*, 1622–1640, 1983.

Firing, E., and R. Lukas, Sampling and aliasing during the NORPAX Hawaii-to-Tahiti Shuttle Experiment, *J. Geophys. Res.*, *90*, 11,709–11,718, 1985.

Goldenberg, S. B., and J. J. O'Brien, Time and space variability of tropical Pacific wind stress, *Mon. Weather Rev.*, *109*, 1190–1207, 1981.

Hayes, S. P., A comparison of geostrophic and measured velocities in the Equatorial Undercurrent, *J. Mar Res.*, *40*, suppl., 219–229, 1982.

Inoue, M., J. J. O'Brien, W. B. White, and S. E. Pazan, Interannual variability in the tropical Pacific Ocean for the period 1979–1982, *J. Geophys. Res.*, *92*, 11,671–11,679, 1987.

Kessler, W. S., and B. A. Taft, Dynamic heights and zonal geostrophic transports in the central tropical Pacific during 1979–1984, *J. Phys. Oceanogr.*, *17*, 97–122, 1987.

Kessler, W. S., B. A. Taft, and M. J. McPhaden, An assessment of the XBT sampling network in the central Pacific Ocean, *Tech. Rep.*

USTOGA4, 62 pp., Univ. Corp. for Atmos. Res., Boulder, Colo., 1985.

Legeckis, R., W. Pichel, and G. Nesterczuk, Equatorial long waves in geostationary satellite observations and in multichannel sea surface temperature analysis, *Bull. Am. Meteorol. Soc., 64*, 133–139, 1983.

Levitus, S., Climatological atlas of the world ocean, *NOAA Prof. Pap. 13*, 173 pp., U.S. Government Printing Office, Washington, D. C., 1982.

McPhaden, M. J., A. J. Busalacchi, and J. Picaut, Observations and wind-forced model simulations of the mean seasonal cycle in tropical Pacific sea surface topography, *J. Goephys. Res.*, this issue.

Meyers, G., Seasonal variation in transport of the Pacific North Equatorial Current relative to the wind field, *J. Phys. Oceanogr., 5*, 442–449, 1975.

Munk, W., Internal waves and small scale processes, in *Evolution in Physical Oceanography*, pp. 264–291, MIT Press, Cambridge, Mass., 1981.

National Academy of Sciences, *U.S. Participation in the TOGA Program—A Research Strategy*, 24 pp., National Academy Press, Washington, D.C., 1986.

Rebert, J. P., J. R. Donguy, G. Eldin, and K. Wyrtki, Relations between sea level, thermocline depth, heat content and dynamic height in the tropical Pacific Ocean, *J. Geophys. Res., 90*, 11,719–11,725, 1985.

Roed, L. P., and O. M. Smedstad, Open boundary conditions for forced waves in a rotating fluid, *SIAM J. Sci. Stat. Comput., 5*, 414–426, 1984.

Sadler, J. C., and B. J. Kilonsky, Deriving surface winds from satellite observations of low-level cloud motions, *J. Clim. Appl. Meteorol., 24*, 758–769, 1985.

Sadler, J. C., M. A. Lander, A. M. Hori, and L. K. Oda, Tropical marine atlas, II, Pacific Ocean, *Tech. Rep. UHMET 87-02*, Dep. of Meteorol., Univ. of Hawaii, Honolulu, 1987.

Weisberg, R. H., D. Halpern, T. Y. Tang, and S. M. Hwang, M_2 tidal currents in the eastern equatorial Pacific Ocean, *J. Geophys. Res., 92*, 3821–3826, 1987.

White, W. B., G. Meyers, and K. Hasunuma, Space/time statistics of short-term climate variability in the western North Pacific, *J. Geophys. Res., 87*, 1979–1989, 1982.

White, W. B., G. A. Meyers, J. R. Donguy, and S. E. Pazan, Short-term climatic variability in the thermal structure of the Pacific Ocean during 1979–1983, *J. Phys. Oceanogr., 15*, 917–935, 1985.

Wunsch, C., and A. E. Gill, Observations of equatorially trapped waves in sea level variations, *Deep Sea Res., 10*, 449–455, 1976.

A. J. Busalacchi, Laboratory for Oceans, NASA Goddard Space Flight Center, Greenbelt, MD 20771.

M. J. McPhaden, NOAA Pacific Marine Environmental Laboratory, 7600 Sand Point Way N.E., Seattle, WA 98115.

J. Picaut, Groupe SURTROPAC, Office de la Recherche Scientifique et Technique Outre-Mer, Nouméa, New Caledonia.

G. Raymond, School of Oceanography WB-10, University of Washington, Seattle, WA 98195.

(Received May 14, 1987;
accepted January 25, 1988.)